Ion Selectivity Predictions from a Two-Site Permeation Model for the Cyclic Nucleotide-Gated Channel of Retinal Rod Cells

Gregg B. Wells* and Jacqueline C. Tanaka#
*Department of Pathology and Laboratory Medicine and Department of Neuroscience, School of Medicine, and #Department of Pathology, School of Dental Medicine, University of Pennsylvania, Philadelphia, Pennsylvania 19104-6002 USA

ABSTRACT We developed a two-site, Eyring rate theory model of ionic permeation for cyclic nucleotide-gated channels (CNGCs). The parameters of the model were optimized by simultaneously fitting current-voltage (*IV*) data sets from excised photoreceptor patches in electrolyte solutions containing one or more of the following ions: Na^+, Ca^{2+}, Mg^{2+}, and K^+. The model accounted well for 1) the shape of the *IV* relations; 2) the binding affinity for Na^+; 3) reversal potential values with single-sided additions of Ca^{2+} or Mg^{2+} and biionic KCl; and 4) the K_i and voltage dependence for divalent block from the cytoplasmic side of the channel. The differences between the predicted K_i's for extracellular block by Ca^{2+} and Mg^{2+} and the values obtained from heterologous expression of only the α-subunit of the channel suggest that the β-subunit or a cell-specific factor affects the interaction of divalent cations at the external but not the internal face of the channel. The model predicts concentration-dependent permeability ratios with single-sided addition of Ca^{2+} and Mg^{2+} and anomalous mole fraction effects under a limited set of conditions for both monovalent and divalent cations. Ca^{2+} and Mg^{2+} are predicted to carry 21% and 10%, respectively, of the total current in the retinal rod cell at −60 mV.

INTRODUCTION

The level of intracellular calcium in the retinal rod outer segment (OS) controls the gain, kinetics, and adaptation properties of visual transduction through a complex and interacting set of Ca^{2+}-sensitive reactions (Kaupp and Koch, 1992; Yau, 1991). The central role of Ca^{2+} in light adaptation first was demonstrated by showing that adaptation is eliminated if Ca^{2+} movement across the OS plasma membrane is eliminated (Yau and Nakatani, 1985a). Ca^{2+} entry into the OS occurs through cyclic nucleotide-gated ion channels (CNGCs), which constitute the only significant population of ion channels in this membrane. These channels are opened in response to cooperative binding of multiple cGMP molecules at the cytosolic face of the channel (Zagotta and Siegelbaum, 1996). Ca^{2+} efflux occurs through a $Na^+/K^+/Ca^{2+}$ exchanger. Cytosolic Ca^{2+} levels reflect a dynamic balance between these fluxes and the Ca^{2+} buffering capacity of the cytosol. Because the activity of cGMP is highest in the dark, Ca^{2+} influx is also greatest in the dark when the number of open CNGCs is at a maximum (Yau and Baylor, 1989; Kaupp, 1991). Through an enzymatic cascade initiated by light-activated rhodopsin, light reduces cGMP levels by increasing phosphodiesterase activity. As cGMP levels fall, CNGCs close and Ca^{2+} influx is reduced.

Analysis of Ca^{2+} selectivity of the rod CNGC in the context of other cations will lead to a better understanding of the mechanism of Ca^{2+} influx into the OS, although assessment of this selectivity by either reversal potential (E_{rev}) or conductance measurements is difficult. In experiments designed to measure the relative Ca^{2+} permeability of CNGCs, the very small currents recorded under biionic conditions with Ca^{2+} precluded accurate determination of E_{rev} (Colamartino et al., 1991; Tanaka and Furman, 1993). The high channel density in photoreceptors and the small Ca^{2+} currents also preclude single-channel determinations of the Ca^{2+} conductance as an alternative measure of relative selectivity.

Using a two-site, Eyring-type model, we analyzed the permeation of the physiologically relevant ions Na^+, Ca^{2+}, Mg^{2+}, and K^+ through CNGCs in rod photoreceptors. We selected this set of ions to predict cellular currents and the cellular flux of Ca^{2+}. As validation for the model, calculations agreed well with experimental measurements of conductance, E_{rev}, and block by Ca^{2+} and Mg^{2+} from native and heterologously expressed rod CNGCs. The notable exception to the agreement of the model and experiments was the predicted concentration dependence of current block by external divalent cations compared to that observed from heterologously expressed channels containing only the α subunit. Permeability ratios from E_{rev} predictions with the single-sided addition of Ca^{2+} or Mg^{2+} depended on the concentration of divalent ion. Although the fraction of multiply occupied channels was very small, anomalous mole fraction behavior, an indicator of multiple occupancy, was predicted for all four ions under particular combinations of ion species, ion concentrations, and method of measurement (E_{rev} or chord conductance). Although permeation models may not have direct structural interpretations in terms of ion binding sites in the pore, models may provide useful physical insights in terms of cytosolic regulation of the channel,

Received for publication 1 July 1996 and in final form 1 October 1996.
Address reprint requests to Dr. Jacqueline C. Tanaka, Department of Pathology, School of Dental Medicine, Levy Center for Oral Health Research, Room 327, University of Pennsylvania, 4010 Locust Street, Philadelphia, PA 19104-6002. Tel.: 215-898-4769; Fax: 215-898-8380; E-mail: tanaka@athens.dental.upenn.edu.

0006-3495/97/01/127/14 $2.00

subunit composition, and the role of selected residues in ion selectivity.

MATERIALS AND METHODS

Current recording

Many of the experimental data used to optimize the parameters of the two-site model were previously published (Furman and Tanaka, 1990; Tanaka and Furman, 1993). For all experiments, inside-out patches were excised from vertebrate retinas of dark-adapted *Rana pipiens* or *Ambystoma tigrinum*. Solution A, containing 120 mM NaCl, 5 mM HEPES, pH 7.4, and both EDTA and EGTA (2 mM), was initially present on both sides of the patch membrane. Currents were recorded with a Dagan 8900 amplifier and were low-pass filtered at 1 kHz before display and storage. Macroscopic steady-state *IV* relations were determined by stimulating the patch with a linear voltage ramp (260 mV/s) from −90 to +90 mV as previously described (Furman and Tanaka, 1990). The small, linear leakage current was measured in the test solution without cGMP; this current was digitally subtracted from the total current measured in the presence of cGMP.

Divalent test solutions contained 120 mM NaCl and 5 mM HEPES (pH 7.4) with the bath divalent concentration as indicated in each experiment. Activities of the ions were used for all data fitting and model predictions. Activity coefficients for NaCl and KCl were taken from Robinson and Stokes (1968); the activity coefficients for Ca^{2+} in the presence of NaCl were taken from Butler (1968). The activity coefficients of Mg^{2+} were equal to the activity coefficients of Ca^{2+} in the presence of NaCl multiplied by the ratio of Mg^{2+}/Ca^{2+} coefficients in the absence of NaCl (Robinson and Stokes, 1968).

Calculation of relative divalent/sodium permeability

Currents were measured in the presence and absence of saturating concentrations of cGMP. The current near 0 pA, usually from −20 to 20 mV, was digitally averaged and linearized to obtain a best fit to the zero current value or reversal potential, E_{rev}.

The relative permeability of Na^+ and Ca^{2+} after single-sided addition of Ca^{2+} was determined according to the Goldman-Hodgkin-Katz current equation (Eq. 1), which is extended to include permeant divalent cations (Lewis, 1979), and ignoring surface charge effects:

$$\frac{P_{Ca}}{P_{Na}} = \frac{\{[Na_o^+] - ([Na_i^+] \cdot e^{FE_{rev}/RT})\} \cdot (1 + e^{FE_{rev}/RT})}{4([Ca_i^{2+}] \cdot e^{2FE_{rev}/RT} - [Ca_o^{2+}])}. \quad (1)$$

In Eq. 1, P is the ionic permeability, E_{rev} is the reversal potential, F is Faraday's constant, R is the gas constant, T is the temperature in K, $[Na^+]$ and $[Ca^{2+}]$ are the activities of the respective ions, and the subscripts i and o denote cytoplasmic side (inside) and extracellular side (outside). A similar equation was used for Mg^{2+}.

Fitting dose-response data

The apparent binding constants for divalent block and Na^+ conductance were determined by Levenberg-Marquardt nonlinear fitting of the equation

$$\text{Current} = I + B_o \Big/ \left(1 + \left(\frac{c}{K_i}\right)^n\right) \quad (2)$$

where I is the residual current, B_o is the maximum response, K_i is the concentration giving half the response, c is the concentration of the ion, and n is the cooperativity index. Fitting was done using Table Curve 2D (Jandel Scientific).

Extraction of single-channel *IV* curves

Macroscopic currents were recorded in the presence of saturating concentrations of cGMP to maximize the opening probability and minimize the effects of gating on the *IV*. The parameters of the Eyring model were not optimized directly against macroscopic currents. Instead, they were optimized by using estimates of the single-channel *IV*'s after taking into account the equilibrium of the channel between closed and open states and the number of channels in each patch. To obtain these estimates, we followed a procedure similar to one used by Zimmerman and Baylor (1992) in which the open-closed equilibrium in the presence of saturating amount of cGMP is represented as

$$\text{closed} \underset{\beta}{\overset{\alpha}{\rightleftarrows}} \text{open}.$$

The macroscopic current in the hypothetical state of all channels being open (I_{open}) was calculated from the actual macroscopic current (I_{gated}) according to Eq. 3:

$$I_{open} = I_{gated} * \left(\frac{\alpha + \beta}{\alpha}\right). \quad (3)$$

The rate constant α was taken as $1.44 \times 10^4\ s^{-1}$, and the value of β at applied transmembrane voltage V_m was taken as $(3.45 \times 10^3\ s^{-1})$ $\exp(-V_m/123\ mV)$ based on values used by Zimmerman and Baylor (1992).

The relaxation of the voltage dependence of gating according to Eq. 3 did not eliminate all voltage dependence of the $I_{open}V$ plot. Although the single-channel *IV* plots from heterologously expressed bovine retina channels containing only the α subunit are nearly linear (Root and MacKinnon, 1993; Goulding et al., 1993), the open channel *IV*'s from rod channels exhibit weak outward rectification (Ildefonse and Bennett, 1991; Sesti et al., 1995) consistent with the shape seen in the $I_{open}V$'s (Zimmerman and Baylor, 1992). The number of channels in each patch (N) was estimated by dividing I_{open} in symmetrical Na^+ solutions by the corresponding V_m and

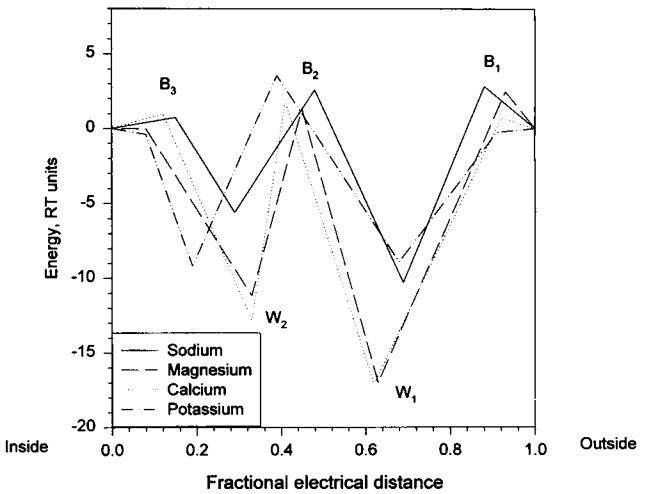

FIGURE 1 Schematic energy diagram of the two-site model for Na^+, Ca^{2+}, Mg^{2+}, and K^+. Barrier and well positions along the ion permeation path are indicated; the energies are given in units of RT for each ion and plotted as a function of the fractional transmembrane electrical distance. The values for energies and fractional positions of the barriers and wells of each ion are given in Table 1.

the single-channel conductance (g) for Na^+:

$$\frac{I_{open}}{g \cdot V_m} = N. \tag{4}$$

Experimentally determined values for g reported for the rod channel vary from 25 to 55 pS (Haynes et al., 1986; Zimmerman and Baylor, 1986; Sesti et al., 1994; Ildefonse and Bennett, 1991; Nizzari et al., 1993). A value of 30 pS was assumed for deriving the single-channel IV curves from the macroscopic $I_{open}V$'s. The number of channels in a patch was assumed not to change with solution changes. Single-channel IV's in the presence of ions other than Na^+ were determined from the same total channel number that was estimated with symmetrical NaCl solutions.

MODEL

Several lines of experimental evidence suggest that the CNGC is a multi-ion pore (Sesti et al., 1995; Furman and Tanaka, 1990; Root and MacKinnon, 1993). We constructed a two-site permeation model based on Eyring rate theory, also known as transition state theory or activated complex theory (Hille, 1992; Eyring, 1935; Eyring et al., 1949). The computational approach is conceptually similar to one described by Begenisich and Cahalan (1980), who used matrix methods for steady-state computation of current as a function of voltage. The Eyring approach provides a useful conceptual framework for computations, although it does not accurately represent details of the physical process of ion transport (Cooper et al., 1988). Energy and distance values, therefore, are best considered as parameters of the model and not as accurate physical measures of the energetics of permeation.

An example of a profile of Eyring parameters that is used in the computations is shown in Fig. 1. The channel in this model contains two local minima in energy, i.e., sites. Each site can be occupied by at most one cation, and an ion can only move into an unoccupied site. The state diagram (Scheme 1) in the case of two ions thus contains nine different states of the open channel. (Scheme 1)

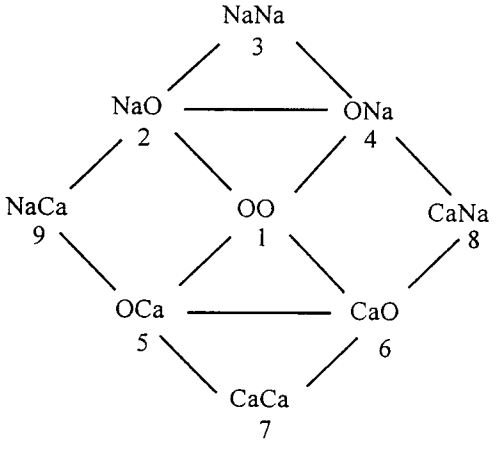

Scheme 1

(5)

Transitions are allowed only between states with a connecting line, leading to 28 forward and reverse rate constants. The general form of the transition matrix is a system of simultaneous equations that describes the probability of any state P_i. Under the steady-state conditions of $dP_i/dt = 0$, the system of equations can be written in matrix form:

$$\begin{bmatrix} -\sum_{j\neq 1}^{9} k_{1j} & k_{21} & \cdots & k_{81} & k_{91} \\ \vdots & \vdots & \vdots & \vdots & \vdots \\ k_{18} & k_{28} & \cdots & \sum_{j\neq 8}^{9} k_{8j} & k_{98} \\ 1 & 1 & \cdots & 1 & 1 \end{bmatrix} \begin{bmatrix} P_1 \\ \vdots \\ P_9 \end{bmatrix} = \begin{bmatrix} 0 \\ \vdots \\ 1 \end{bmatrix}. \tag{6}$$

The rate constants k_{ij} (i = initial state, j = final state), without considering ion-ion interaction, are functions of the parameters of the Eyring energy profile shown in Fig. 1. For example,

$$k_{21} = A \cdot \exp(-(B_1 - W_1)) \cdot \exp(-(dW_1 - dB_1) \cdot zFV_m/RT), \tag{7}$$

where A is a preexponential factor, V_m is the applied transmembrane voltage, B_1 is the first barrier, W_1 is the first well, and dB_1 is the distance of the first barrier, and so on.

The appropriate range of values for A depends on whether the transition is bimolecular or unimolecular. The bimolecular reactions of this model occur when a cation from the solution and the ion channel combine to form a unimolecular complex. Such reactions, for example, are described by the rate constants k_{12} and k_{14}. The value of A depends on the partition functions of the species involved in the reaction and that of the activated complex (Moore and Pearson, 1981); therefore, the value of A for the bimolecular reactions was optimized independently for different ions. For an atom and nonlinear molecule as reactants, the value of A is in the range of 10^8–10^9 (Moore and Pearson, 1981; Jencks, 1987). Transitions originating with a cation-channel complex are unimolecular, with A fixed at kT/h.

The effects of electrostatic ion-ion interactions are incorporated into the model as additive shifts in the energy wells and barriers around an occupied site that are equal in RT units to the product of the charges, the inverse of the distances from that occupied site, and a proportionality factor A_{inter}. Electrical distances were independent of the number of ions occupying the channel. This technique has been used by Alvarez et al. (1992) for Eyring models of permeation. A reasonable starting value for A_{inter} can be determined from a calculation for monovalent ions whose interaction energy within a finite pore depends on the distance between ions and the dielectric effects of the bath, channel pore, and membrane, but neglects the dielectric effect of the channel protein (Levitt, 1978). For a distance of 0.5 units between sites in fractional space and 12.5 Å in real space within a pore with a overall length of 25 Å, the energy of interaction between unit charges according to this method of calculation is $3RT$. This energy leads to a reasonable starting value of A_{inter} of $1.5RT$ before optimization. The same value of A_{inter} after optimization was used for all ions.

The current of a particular ion is its steady-state net flux crossing over any one barrier multiplied by its valence. If the middle barrier is selected, then the fluxes and currents for Na^+ and Ca^{2+}, for example, are

$$\text{Flux } Na^+ = P_2 \cdot k_{24} - P_4 \cdot k_{42} = \text{Current } Na^+$$
$$\text{Flux } Ca^{2+} = P_6 \cdot k_{65} - P_5 \cdot k_{56} = (\text{Current } Ca^{2+})/2. \tag{8}$$

The values of P_i are found by solving the matrix equation 6. The total current is the sum of the fluxes of all ions multiplied by their valences.

Extension of this model to four ions is straightforward. For four different ions, there are 88 nonzero transitions and 25 different states for the two-site model containing 0, 1, or 2 ions. The construction of a state diagram similar to Scheme 1 and a transition matrix similar to Eq. 6 is straightforward. This four-ion model was used to predict IV curves for pseudocellular ionic concentrations.

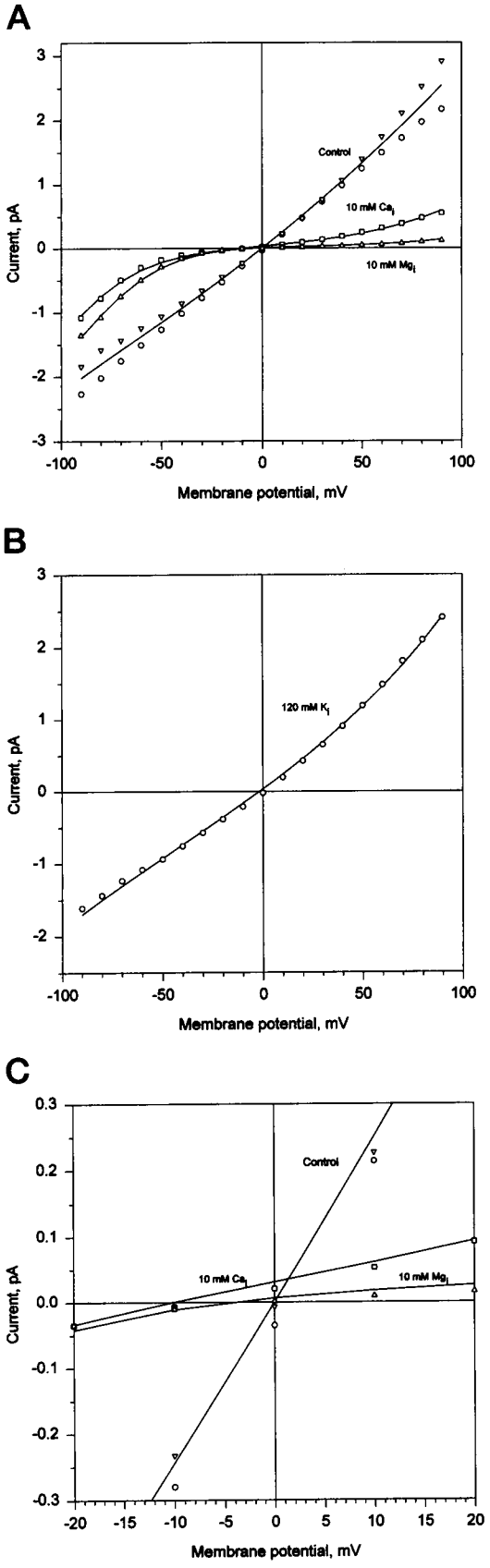

FIGURE 2 Derived single-channel *IV* data and *IV*'s from the two-site model for the major physiological ions. Macroscopic *IV*'s were recorded from two patches with saturating cGMP concentrations and symmetrical 120 mM NaCl solutions in the absence of divalent cations. The single-channel current from each patch was determined by relaxing the voltage dependence of the *IV* relation and dividing the macroscopic current by the estimated number of channels in the patch as described in Materials and Methods. Macroscopic *IV*'s from a patch were recorded in solutions containing 120 mM NaCl and either 10 mM $CaCl_2$ or 10 mM $MgCl_2$ on the inside (cytoplasmic), and the single-channel *IV*'s were derived using the estimated channel number for that patch. Biionic KCl macroscopic currents were recorded from a second patch, and the single-channel currents were similarly derived. Data are shown with symbols. The model predictions derived from simultaneous parameter optimization of these five data sets from two patches are shown as solid lines. (*A*) Data and predicted currents for symmetrical 120 mM NaCl and symmetrical 120 mM NaCl with single-sided addition of either 10 mM Ca_i^{2+} or Mg_i^{2+}. The two control *IV*'s from two different patches (○, ▽) are nearly linear, with the zero current crossing at 0 mV. In the presence of cytoplasmic Ca^{2+} (□) or Mg^{2+} (△), currents show voltage-relieved block at potentials less than −40 mV. The inward current shows more block with Ca^{2+} than Mg^{2+}; however, Mg^{2+} blocks the outward current more strongly (b0523, 510 channels). (*B*) Data and predicted current for biionic KCl. The overall shape of the *IV* is similar to that for NaCl and the reversal potential is close to 0 mV (b79242k, 444 channels). (*C*) Reversal potentials from A. Reversal potentials determined from the data were −8.0 mV and −0.23 mV, respectively. The reversal potentials fitted by the model under these ionic conditions were −10.5 mV and −0.48 mV, respectively. The E_{rev}'s from the data were determined by fitting the currents at potentials near zero; values of −8.0 and −0.48 mV were found for 10 mM Ca^{2+} and Mg^{2+}, respectively. The model predicted E_{rev}'s of −10.5 and −0.48 mV.

The reference state corresponds to a standard state of 1 M. The temperature used throughout is 300 K. The model does not explicitly incorporate the effects of surface charges or effects of the electric field from the channel. All computations involving the model, including nonlinear optimization of parameters with a Levenberg-Marquardt algorithm (Marquardt, 1963) and calculations of currents, reversal potentials, permeability ratios, and anomalous mole fraction effects, were performed with the software package Matlab (MathWorks, Natick, MA). The reversal potentials were found numerically using a combination of bisection, secant, and inverse quadratic interpolation methods (Forsythe et al., 1976).

RESULTS

Model parameters

Macroscopic currents were transformed into single-channel data as described in Materials and Methods. These derived *IV*'s were used to optimize the parameters of the model as shown in Fig. 2, *A* and *B*. The derived single-channel Na^+ currents in divalent-free solutions exhibited weak outward rectification (Fig. 2 *A*). When divalent cations were added to the bath (cytosolic face), the outward currents were blocked. Mg^{2+} is a more effective blocker of outward currents than Ca^{2+} at 10 mM concentrations. Inward currents were also blocked by the addition of divalent cations to the internal side of the membrane, but the block is partially relieved at potentials more negative than −40 mV. The *IV* measured in biionic KCl (Fig. 2 *B*) was similar to the shape recorded in symmetrical NaCl solutions.

Optimization of the parameters using the data in Fig. 2 required several steps. First, nondistance parameters for each ion (energies, interaction energy, and preexponential factors) were varied with fixed symmetrical distances. Next,

the distances and nondistance parameters were optimized simultaneously. The distances then were fixed at the new values, and the nondistance parameters were reoptimized. Finally, a hypothetical data set that represented the shape of experimental *IV*'s (Zimmerman and Baylor, 1992; Matthews, 1986; Yau et al., 1986) in the presence of pseudo-physiological ion concentrations (Na_i^+ = 6, Na_o^+ = 120; K_i^+ = 2.5, K_o^+ = 120; Ca_i^{2+} = 10^{-7} M, Ca_o^{2+} = 1.5; Mg_i^{2+} = 0.3, Mg_o^{2+} = 6) was included in the parameter optimization. This optimized set was used for all subsequent computations and is presented in Table 1.

The Eyring profile of the two-site model for all ions is shown in Fig. 1. We attempted to include in the fitting multiple data sets from additional patches at other concentrations of divalents to constrain the set of model parameters. The patch-to-patch variability was too large to further constrain the parameters. Haynes (1995b) found similar patch-to-patch variability when examining the effects of intracellular divalent cations on cone patches. We elected to fit five data sets from two representative patches. Although other parameter sets may fit these data, we selected this optimized parameter set as the working model for investigating the selectivity properties of the CNGC.

The inner and outer wells are located at slightly asymmetrical electrical distances of 20–35% and 60–70% through the membrane field. The barriers are lower for Ca^{2+} than for either Na^+ or Mg^{2+}, particularly the outside barrier B_1. The wells for both Ca^{2+} and Mg^{2+} are much deeper than for Na^+, as expected on the basis of the current block in the presence of these divalent cations. The wells for Ca^{2+} are slightly deeper than for Mg^{2+}. The tight association of divalent cations with the channel prolongs their transit time compared to that of Na^+ and restricts the flow of Na^+ current, seen experimentally and computationally as current block by these divalent cations.

The *IV* predicted for symmetrical Na^+, shown as a solid line in Fig. 2 *A*, falls between the currents recorded in the absence of divalent cations from two patches. Patch-to-patch variability (Karpen et al., 1993; Zimmerman and Baylor, 1986) in the shape of the macroscopic *IV*'s under symmetrical Na^+ conditions likely reflects relevant physiological factors such as subunit heterogeneity and modification of the channel properties by phosphorylation or glycosylation (Yau and Chen, 1995; Zagotta and Siegelbaum, 1996). Fig. 2 *C* shows good agreement of the model with measured reversal potentials, E_{rev}, in the presence of the divalent cations.

Conductance as a function of [Na^+]

Parameters for the model were determined using a single concentration of Na^+. An initial test of the accuracy of the model was the prediction of Na^+ conductance across a range of Na^+ activities for which experimental data were available. The conductance was predicted as a function of the thermodynamic driving force $V_m - E_{rev}$ at Na^+ activities from 10 μM to 10 M. The predicted conductance versus activity values were fitted using Eq. 7 and are shown with the solid line in Fig. 3 for $V_m - E_{rev}$ = 40 mV. The calculated K_i for Na^+ activity was 6.3 mM. The predicted conductances show good agreement with data taken from a single patch exposed to different concentrations of Na^+ in the bath (Furman and Tanaka, 1990). Higher K_i values of 249 mM (~180 mM activity) at +90 mV (Menini, 1990) and 180 mM (~142 mM activity) at +90 mV (Zimmerman and Baylor, 1992) have also been reported; however, these values were determined using the V_m, without considering the thermodynamic driving force.

Divalent block of CNGCs

The fraction of unblocked current as a function of membrane potential is shown in Fig. 4. The left panels show the effects of adding internal divalent cations, and the right panels show the effects of external divalent additions. Predictions from the model at 1 mM and 10 mM concentrations are indicated by the solid lines. Data from Fig. 2 *A* are shown by the symbols in the left panels. Block is steeply voltage dependent for inward currents with the addition of internal divalent cations, with little voltage dependence for outward currents. For the addition of external divalent cations, the inward currents show little voltage dependence, with the outward currents showing voltage-relieved block. The major difference between the effect of internal Ca^{2+} and Mg^{2+} is the more effective blocking ability of Mg^{2+} of the outward currents, especially at 1 mM concentrations.

TABLE 1 Optimized parameter set

Ion	B_1^*	B_2	B_3	$W_1^\#$	W_2	$dB_1^\S$	dB_2	dB_3	dW_1	dW_2	$A^\P$
Na^+	2.83	2.59	0.73	−10.30	−5.60	0.88	0.48	0.15	0.69	0.29	3.63
Ca^{2+}	0.72	1.81	1.00	−17.12	−12.80	0.92	0.41	0.12	0.62	0.33	5.50
Mg^{2+}	2.48	1.30	−0.027	−17.0	−11.17	0.93	0.45	0.08	0.63	0.33	3.24
K^+	−0.24	3.56	−0.40	−8.90	−9.18	0.91	0.39	0.08	0.68	0.19	4.34

* Energy height of barrier in *RT* units.
\# Energy depth of well.
§ Fractional distance of barrier or well from the inside.
¶ Preexponential factor × 10^9.
A_{inter} = 2.98 (proportionality factor for interaction energy for all ions).

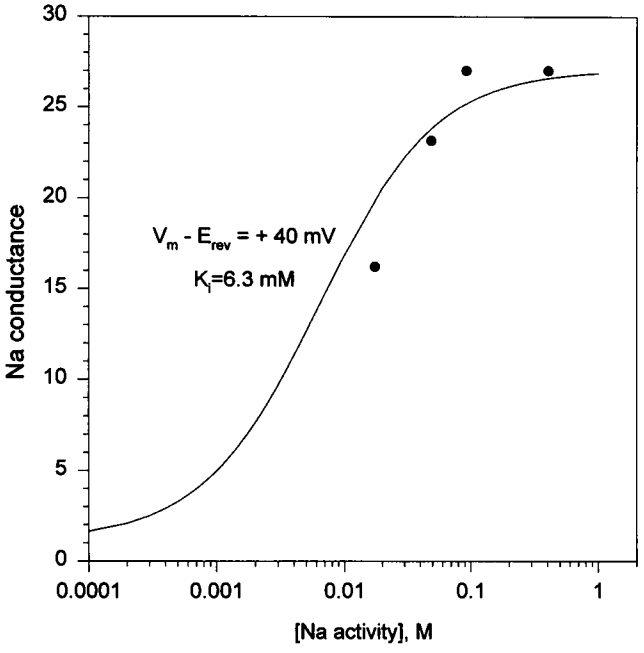

FIGURE 3 Sodium conductance as a function of Na^+ activity. The solid lines are Na^+ conductances predicted at +40 mV from the model, with Na^+ concentration in the bath varying from 0.1 mM to 10 M and 120 mM NaCl in the pipette, similar to conditions used in previous experiments. The solid curve is the conductance calculated from the thermodynamic driving force, $V_m - E_{rev} = +40$ mV and fitted with a nonlinear fitting algorithm (Eq. 2). A best fit gave a K_i value of 6.3 with an n value of 0.95. Data from a patch exposed to multiple Na^+ concentrations are shown by the symbols.

K_i values of block were determined for the addition of divalent cation at each membrane face by using Eq. 2. Examples of plots of the current versus activity of Ca^{2+} or Mg^{2+} at −80 mV are shown in the left panels in Fig. 5. The predicted K_i values taken from such plots are shown as a function of voltage on the right panels in Fig. 5. The K_i for Ca_i^{2+} decreases between −90 mV and +20 mV until it reaches a limiting value of about 1 mM. The predicted K_i at +60 mV for Ca_i^{2+} agrees well with the value determined by Karpen et al. (1993). The K_i for Mg_i^{2+} shows a greater range as it decreases steadily between −90 mV and +20 mV to reach a limiting value of about 0.1 mM above +30 mV. Again, the predicted K_i at +40 mV for Mg_i^{2+} agrees well with the value from Karpen et al. Other reported values of K_i from measures of the concentration dependence of block by Ca^{2+} and Mg^{2+} from the cytoplasmic face vary from the predictions of the model by at most 2.5 times (Colamartino et al., 1991; Zimmerman and Baylor, 1992; Tanaka and Furman, 1993).

Similar computations were used to predict the blocking ability of external Ca^{2+} and Mg^{2+}. The left panels of Fig. 5 show that the K_i for Ca_o^{2+} is less than 0.1 mM at −90 mV. Its value increases when the driving force is increased from −30 mV to 90 mV, where it reaches a value of about 2 mM. The K_i for Mg_o^{2+} starts out at 1 mM, higher than that of Ca_o^{2+}. It remains constant until +20 mV and then increases slightly to reach 4 mM at +90 mV. The index of cooperativity, n, obtained from fitting Eq. 2 ranges from 0.6 to 1.0 at −80 mV, suggesting that occupancy of one of the binding sites by a divalent cation is sufficient to block Na^+ current.

K_i values for externally applied Ca^{2+} have not been measured in photoreceptor patches because of the difficulty of obtaining stable outside-out seals (Haynes, 1995b). K_i values are available, however, from Park and MacKinnon (1995) on outside-out patches from heterologous expression of retina CNGC α subunits in *Xenopus* oocytes. Data points from these experiments are shown at −30 mV for both Ca_o^{2+} and Mg_o^{2+}. Similar values for external divalent block were reported by Eismann et al. (1994) and Root and MacKinnon (1993). In contrast with the good agreement between predictions and measurements of cytoplasmic Ca^{2+} and Mg^{2+} block with native retinal channels, there are substantial differences for the K_i's of external Ca^{2+} and Mg^{2+} block between the model predictions and measurements from heterologously expressed channels. The experimental K_i for Ca_o^{2+} is 63-fold higher than the predicted value from the model. For Mg_o^{2+}, the difference is 16-fold higher. These discrepancies may reflect the properties of native CNGCs in contrast to heterologously expressed homomeric channels, because differences in channel gating have been shown for heterologous expression of channels containing the β subunit (Bradley et al., 1994; Chen et al., 1994; Liman and Buck, 1994; Sesti et al., 1996). Experimentally, this issue can be addressed by examining divalent block in heterologously expressed channels containing either the α subunit alone or the α and β subunits.

In the Eyring formulation, the voltage dependence of the K_i's is a function of the location of a binding site within the electric field (Woodhull, 1973). The linear regions of plots of the log K_i versus V_m give measurements of this fractional electrical distance δ of 0.44, 0.35, 0.43, and 0.41 for Ca_i^{2+}, Mg_i^{2+}, Ca_o^{2+}, and Mg_o^{2+}, respectively. Park and MacKinnon (1995) measured δ as 0.22 and 0.46 for Ca_o^{2+} and Mg_o^{2+}, respectively. Once again, predictions of the model vary from the experimental measurements on heterologously expressed CNGCs for Ca_o^{2+} block.

Relative cationic selectivity of CNGCs

The ionic selectivity of CNGCs is physiologically important because Ca^{2+} influx through these channels into the OS plays a central role in light adaptation by rod photoreceptors. The selectivity characteristics of CNGCs also serve as a point of comparison among members of the CNGC family, especially those closely related members from rods, cones, and olfactory neurons. These three channel types have very similar sequences in the conserved P region known to be involved in ion selectivity in these channels, and yet their permeation properties for Ca^{2+} differ significantly (Picones and Korenbrot, 1992; Haynes, 1995b; Frings et al., 1995). In the following section, we examine various predictions of divalent selectivity for the photoreceptor channel and, where data are available, compare the predictions to experimental results.

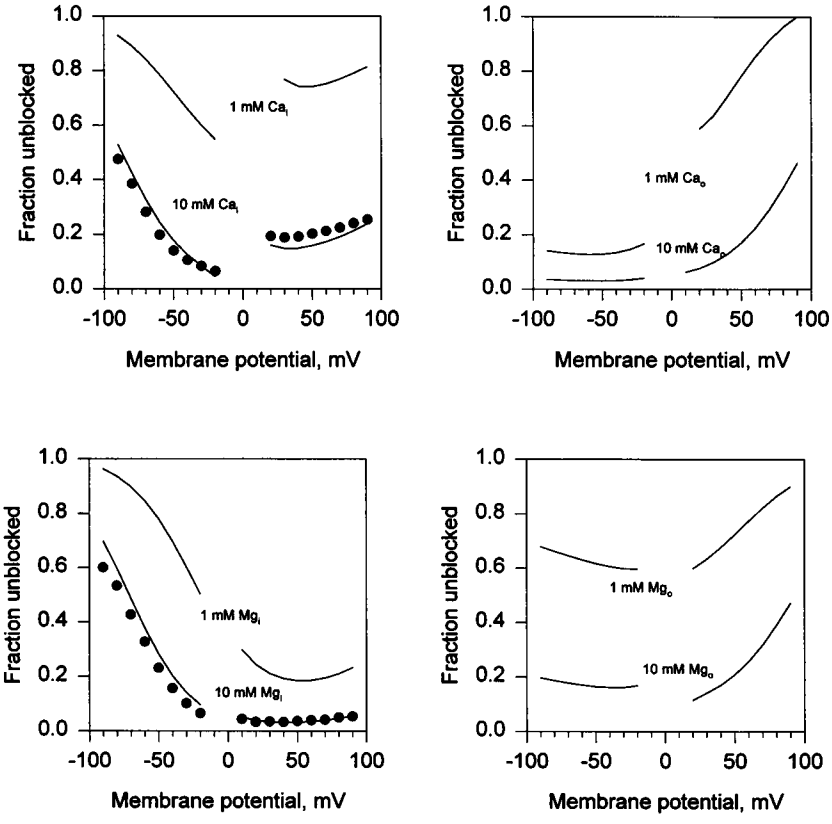

FIGURE 4 Voltage dependence of divalent block from both sides of the membrane. The fraction of unblocked current was predicted from the model as a function of the transmembrane potential with either 1 or 10 mM divalent cations added to either side of the membrane. Data from the *IV*'s in Fig. 2 are shown by the symbols. When divalent cations are added to the internal side of the membrane, the outward current block is nearly voltage independent. Inward currents show increasing relief from block as the absolute potential is increased. Similarly, inward currents are blocked when divalent cations are present on the outside. The small currents near 0 mV in the absence of divalent cations often result in discontinuities when the fraction of unblocked current is calculated. To avoid these discontinuities, these potentials were eliminated from the plots.

The relative selectivity of an ion channel for permeant ions can be characterized by two different measures: E_{rev} and conductances (Hille, 1975; Eisenman and Horn, 1983). E_{rev} is the transmembrane voltage at which the unidirectional ion influx equals the efflux; it is independent of gating effects and channel number. E_{rev} in the presence of two permeant species, one of which is divalent and one monovalent, operationally defines their permeability ratio according to Eq. 1. Experimentally, permeability ratios may depend on the orientation of permeant species relative to the defined topology of the membrane and on the absolute concentration of the ions. The second measure, conductance, is the net rate of ion transport across the membrane through the open channel. Like other transport phenomena, conductance displays competition, block, and saturation effects with changes in the ionic composition.

The CNGC from rods is relatively nonselective for monovalent cations in the absence of divalent cations, a characteristic that is apparent from the *IV* in Fig. 2 *B* with biionic KCl replacement. Because the experimental E_{rev} shift is very nearly zero, it can be recognized immediately that the relative permeability ratio P_K/P_{Na} is very nearly 1. The average measured E_{rev} was 1.5 mV (± 1.2 mV, n = 11), resulting in a P_K/P_{Na} of 0.93 (Furman and Tanaka, 1990). The predicted E_{rev} from the model is −1.92 mV, resulting in a P_K/P_{Na} of 1.08. The relative conductance for K^+ compared to Na^+, based on the predicted single-channel currents from the model at +60 mV, is 0.90. Although there is no direct experimental comparison from single-channel currents, this value compares well with a previous determination of 0.79 based on macroscopic currents in biionic KCl (Furman and Tanaka, 1990).

The single-sided addition of Ca_i^{2+} on the cytoplasmic side produces a measurable negative shift in the E_{rev}, implying that Ca^{2+} is more permeant than Na^+ (Fig. 2 *C*). The experimentally determined E_{rev}'s in Fig. 2 *C* were −8.0 and −0.23 mV for Ca^{2+} and Mg^{2+}, respectively. The average E_{rev} value with 10 mM Ca_i^{2+} was −10.4 mV (±1.9, n = 7). For Mg_i^{2+}, the average was −1.75 mV (n = 3). The E_{rev} predicted with 10 mM Ca_i^{2+} and Mg_i^{2+} were −10.5 and −0.48 mV, respectively. E_{rev} shifts predicted for single-sided additions of Ca^{2+} or Mg^{2+} to either side of the membrane are plotted as a function of divalent activity in Fig. 6 *A*. Significant shifts in E_{rev} are only seen at divalent activities above several mM for Ca_i^{2+}. Significant shifts with Mg_i^{2+} require even higher concentrations.

Fig. 6 *B* displays permeability ratios that are calculated from the E_{rev} shifts. The P_{Ca}/P_{Na} determined from the average E_{rev} at 10 mM Ca_i^{2+} is 5.2 indicated by the single data point; the P_{Mg}/P_{Na} ratio is 0.92. This value is about half of the predicted value. The confidence in this experimental measurement is low, however, because the E_{rev} is near 0 mV and determining the actual zero current crossing is difficult with the small magnitude of currents in the presence of Mg_i^{2+}. Picones and Korenbrot (1995) recently examined the relative permeabilities of both rod and cone photoreceptors using a similar experimental approach. They estimated a somewhat lower P_{Ca}/P_{Na} of 3.1 in rods with 10 mM Ca_i^{2+}.

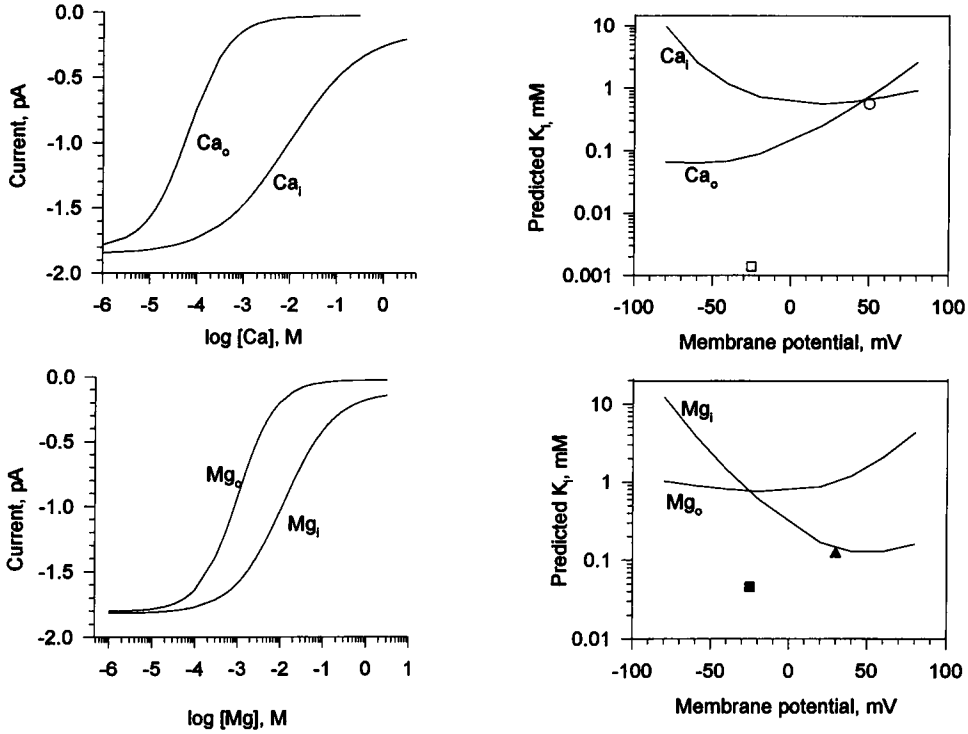

FIGURE 5 Voltage dependence of divalent K_i values. (*Left panels*) K_i as a function of external and internal divalent cations added to 120 mM symmetrical NaCl solutions. Predicted currents were plotted for −80 mV over a range of divalent ion concentrations to determine the K_i values for divalent block using Eq. 7. The K_i (in mM) and n values were 9.7 and 0.6 for Ca_i^{2+}; 0.066 and 1.0 for Ca_o^{2+}; 12.3 and 0.75 for Mg_i^{2+}; and 1.02 and 1.0 for Mg_o^{2+}. (*Right panels*) Divalent K_i values as a function of voltage. K_i values were calculated at each potential and plotted as a function of the membrane potential. Data points were selected from published values as follows: Ca_i^{2+} (○) taken from Karpen et al. (1993); Ca_o^{2+} (□) taken from Park and MacKinnon (1995); Mg_i^{2+} (▲) taken from Karpen et al. (1993); and Mg_o^{2+} (■) taken from Park and MacKinnon (1995). The voltage dependence of the K_i values was determined from the slope of the log K_i versus V_m over the linear range. The slopes for Ca^{2+} and Mg^{2+} added to the external side of the membrane were 1.46×10^{-4} mV^{-1} and 1.39×10^{-4} mV^{-1}, giving a fractional electrical distance of 0.43 and 0.41, respectively, according to the equation $K_i = K_i(0\ mV)\exp(z\delta FV_m/RT)$ (Woodhull, 1973). Slopes for the voltage dependencies of divalent cations from the cytoplasmic side were -1.86×10^{-2} mV^{-1} and -2.17×10^{-2} mV^{-1}, respectively. δ's are 0.44 and 0.35, respectively.

We also predicted the relative selectivity for Ca^{2+} and Mg^{2+} based on conductance, although these determinations have been inaccessible experimentally because of the small divalent currents in pure divalent solutions. The predicted single-channel currents at +60 mV with 120 mM Na^+ and 60 mM Ca^{2+} or Mg^{2+} were 1.61, 0.125, and 0.027 pA for Na^+, Ca^{2+}, and Mg^{2+}, resulting in conductances at +60 mV of 26.8, 2.08, and 0.45 pS, respectively. The relative conductances compared to Na^+ were 0.078 and 0.017 for Ca^{2+} and Mg^{2+}; estimated relative conductances based on macroscopic currents in biionic solutions were 1:0.012:0.004 (Colamartino et al., 1991).

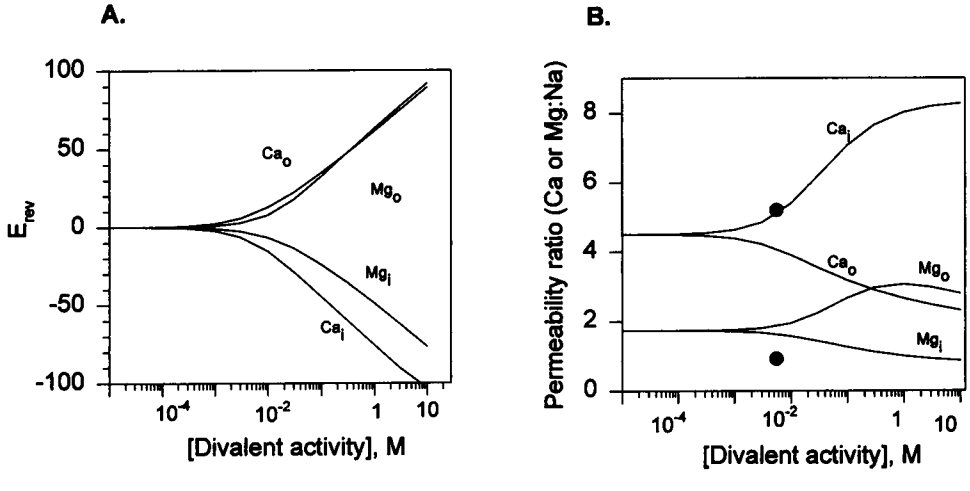

FIGURE 6 (*A*) E_{rev} as a function of divalent ion concentrations. E_{rev} values were predicted for solutions containing Ca^{2+} or Mg^{2+} added to either side of the membrane in the presence of symmetrical 120 mM Na^+. o, outside; i, inside. (*B*) Permeability ratios as a function of divalent ions from either side of the membrane. The Ca^{2+}:Na^+ and Mg^{2+}:Na^+ ratios were calculated from E_{rev} shifts according to Eq. 6 as the divalent concentrations were increased from 10^{-5} M to 10 M. The experimentally determined permeability ratios based on the data in Fig. 2 *B* with 10 mM internal Ca^{2+} or Mg^{2+} are shown by the solid symbols.

Calculated populations from the model

The permeation properties of the model depend on the relative population of each state shown in Scheme 1. These populations are a function of voltage and ionic concentrations. In Eyring models of the Ca^{2+} channel, for example, the fraction of states doubly occupied with Ca^{2+} increases with increasing Ca^{2+} concentration, accounting for the high Ca^{2+} conductance (Campbell et al., 1988). We examined the relative population of each of the states in the model to explain the small conductance of Ca^{2+} through the CNGC.

At 120 mM symmetrical Na^+ and 10 mM Ca^{2+} on the cytoplasmic side, the relative occupancies in Fig. 7 *A* of the available states shown in Eq. 5 depend on V_m. When singly occupied Ca^{2+} states (i.e., CaO + OCa) predominate between −40 and +70 mV, the channel is blocked. At more extreme positive and negative voltages, singly occupied Na^+ states (i.e., NaO + ONa) predominate, and the block is relieved. Less than 10^{-4} of the channel population contains two Na^+ ions. Double occupancy involving Ca^{2+} states is much more rare. The fraction of (CaNa + NaCa) is about 10^{-7}; the fraction of CaCa is about 10^{-15}.

Fig. 7 *B* shows the relative occupancy of the predominating available states as a function of concentration of added Ca^{2+} at a constant driving force of +40 mV. The (NaO + ONa) states predominate below the K_i for Ca^{2+}. Again, double occupancy is rare. The fraction of (CaNa + NaCa) always is less than 10^{-7} across all concentrations in Fig. 7 *B*; the fraction of CaCa is always less than 10^{-15}.

Anomalous mole fraction effect

The first experimental evidence that CNGCs are multi-ion channels was the observation that E_{rev} shifts for Na^+/NH_4^+ and Na^+/Cs^+ in biionic solutions depend on the absolute concentration of cations (Furman and Tanaka, 1990). Another diagnostic feature of multi-ion channels is anomalous mole fraction (AMF) effects (Hille, 1992). Attempts to measure AMF effects using mixtures of Na^+ and Ca^{2+} were unsuccessful (Zimmerman and Baylor, 1992), but recently Sesti et al. (1995) reported AMF effects using mixtures of Li^+/Cs^+. AMF effects, in principle, can be observed through either E_{rev} or conductance measurements at a constant thermodynamic driving force. Observation of AMF effects depends on the ion species, the range of concentrations used, and the method of observation (E_{rev} or conductance) (Hille and Schwarz, 1978; Campbell et al., 1988).

Scanning for AMF effects with the four physiological ions across different conditions is straightforward with the model. An AMF effect can be identified by calculation of the limiting values of the slope of the graph of E_{rev} or conductance as a function of mole fraction of one of the ions. If an AMF effect is present, the slope at the left-hand side of the graph must have a sign that is opposite that of the slope at the right-hand side. First we looked at the AMF effect with Ca^{2+}/Mg^{2+}, with total divalent ion activities ranging from 10 nM to 50 M. This range of activities was much wider than was used to parameterize the model; however, we extrapolated over this range to examine the

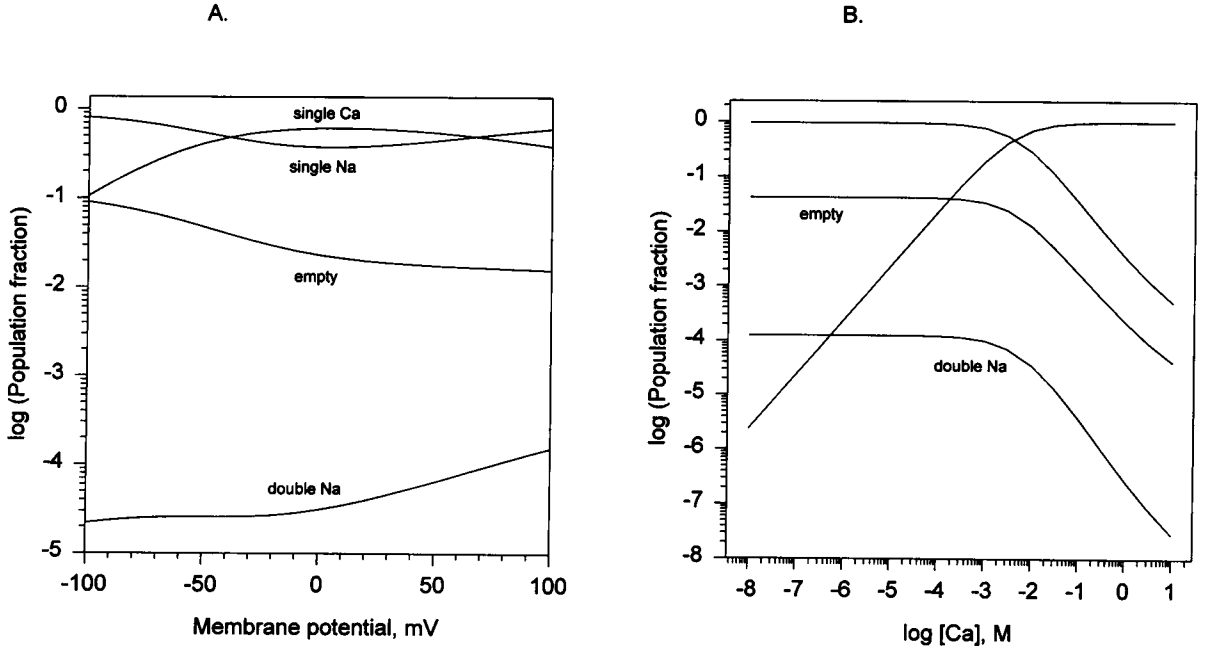

FIGURE 7 Effect of calcium on the channel occupancy as a function of membrane potential and calcium concentration. (*A*) Predicted fractions of the channel population in the empty, single Na^+, single Ca^{2+}, and double Na^+ states are plotted as a function of membrane potential with Na^+ at 120 mM and Ca_i^{2+} at 10 mM concentration. At large negative voltages, the channel is mostly occupied by a single Na^+ ion. With increasing voltage, the single Ca^{2+} states predominate, and the fraction of the NaNa state begins to increase. Above about +65 mV, the single Na^+ states again predominate over the single Ca^{2+} states. The calculated fraction of the CaCa state is less than 10^{-10} at all potentials. (*B*) Predicted fractions of the same states are plotted as a function of cytoplasmic Ca_i^{2+} with 120 mM Na^+ at +40 mV. The fraction of single Ca^{2+} states becomes significant at about 1 mM, as expected from the plot of K_i shown in Fig. 5. The fraction of CaCa is less than 10^{-10}, even at the largest concentration of Ca_i^{2+} used for the calculation.

behavior of the CNGC that is predicted by the model. No AMF effect for E_{rev} was predicted across this activity range with either Ca^{2+} or Mg^{2+} alone on the cytoplasmic side and a mixture of Ca^{2+}/Mg^{2+} at the same constant total activity on the extracellular side. Likewise, no AMF effect on E_{rev} was predicted with the ionic conditions reversed with respect to the membrane, i.e., with the single divalent ion on the extracellular side and the same total activity of divalent mixture on the cytoplasmic side. In contrast, the chord conductance at +80 mV total driving force showed an AMF effect when Ca_i^{2+}/Mg_i^{2+} was present at 0.1 M total divalent ion activity against Na_o^+ at 0.092 M. The AMF effect was not predicted at lower total activities of divalent cations.

Second, we looked at the E_{rev} for the monovalent ions across the same range of concentrations (Fig. 8). In contrast to the divalent ions, an AMF effect is predicted for Na^+ on the extracellular side and a mixture of Na^+/K^+ on the cytoplasmic side at 1 M total ion concentration and greater. The range of shift in E_{rev}, however, is very small. The AMF effect was abolished at 0.5 M and less, illustrating the sensitivity of the effect to the total ion concentration.

Just as AMF effects have been taken to imply multisite channel models, their absence has also been taken to imply single-site models. The absence of such effects must be interpreted carefully because of the sensitivity of AMF effects to the conditions of ion species, total ion concentration, use of E_{rev} or conductance for the measurements, and the choice of driving voltage when measuring conductance. The model suggests that certain conditions do exist under which AMF effects are present. Although we did not attempt to predict such effects with all possible combinations of these variables, the large concentrations with which we detected an AMF effect from the model generally are experimentally inaccessible and the magnitudes of the effect were small. It is not surprising, therefore, that AMF effects have not been reported from experiments with combinations of Na^+, Ca^{2+}, Mg^{2+}, and K^+.

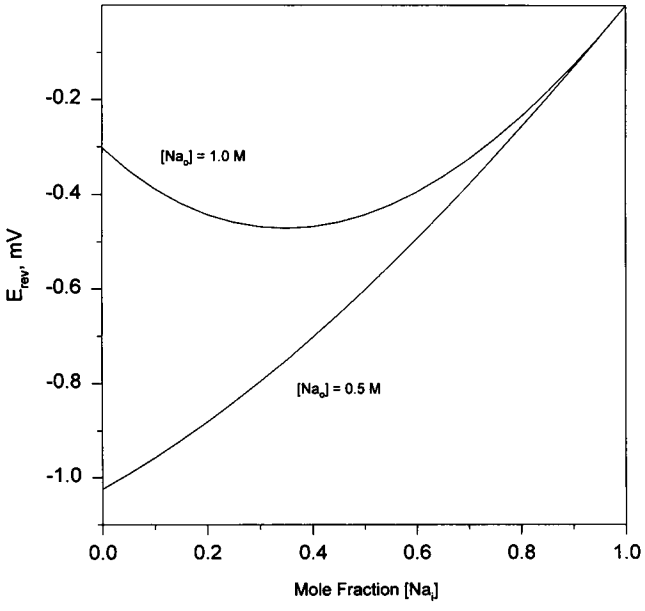

FIGURE 8 Concentration-dependent anomalous mole fraction effects revealed by E_{rev} with Na^+ on the outside and Na^+/K^+ on the inside. An anomalous mole fraction effect for E_{rev} is predicted for total ion activities of 1 M and greater with Na^+ on the outside and the mixture of Na^+ and K^+ on the inside. The AMF is clearly seen at 1 M total cation activity, but not at 0.5 M total cation activity.

Predicted cellular currents and fluxes for each ion

Our final goal for studying Na^+, Ca^{2+}, Mg^{2+}, and K^+ under relatively simple ionic conditions was to predict total and ion-specific currents under more complex, physiological conditions with multiple ions present on both sides of the membrane. Because the contribution of a single species within a mixture to the total current cannot be identified with electrophysiology, modeling of ion fluxes will help predict the effects of ion-specific currents on cell physiology.

Results of modeling the *IV* of the OS in the presence of Na^+, Ca^{2+}, Mg^{2+}, and K^+ at physiological concentrations are presented in Fig. 9 *A*. The *IV* shows a pronounced outward rectification, similar to the overall shape of the in vivo *IV* of the light-activated current (Zimmerman and Baylor, 1992). The ratio of Ca^{2+} and Mg^{2+} current to Na^+ current and the total current are shown in Fig. 9 *B*. The fraction of total current carried by Ca^{2+} at −60 mV is 21%; for Mg^{2+} it is 10%. This prediction agrees well with estimates in the literature of 15–25% for Ca^{2+} (Nakatani and Yau, 1988; Perry and McNaughton, 1991) and 5% for Mg^{2+} (Nakatani and Yau, 1988). Fig. 9, *C* and *D*, shows the flux versus voltage for each ion. Near −50 mV, the region important for cell signaling, the ratio of Ca^{2+} to Na^+ decreases with depolarization, although the fraction of Ca^{2+} current compared to the total current is constant. On the other hand, the ratio of Mg^{2+} to Na^+ is constant with depolarization, but the fraction of Mg^{2+} current compared to total current increases.

DISCUSSION

What do we learn from the model?

First, the two-site model predicts Na^+ and K^+ conductances and Ca^{2+} and Mg^{2+} block reasonably accurately. Notable discrepancies between the model and experimental data are the approximately 60-fold difference in the K_i for Ca_o^{2+} block and the difference between the measured and predicted value of δ derived from the voltage dependence of K_i for Ca_o^{2+}. The predicted K_i for external Mg^{2+} differed by 16-fold from the experimental measurement. These experimental values were determined in a heterologous expression system in which only the α subunits from the retina CNGC were expressed (Eismann et al., 1994; Park and MacKinnon, 1995). Although these discrepancies may reflect errors of the model, a more likely explanation is that external divalent interactions, but not internal divalent interactions, are mod-

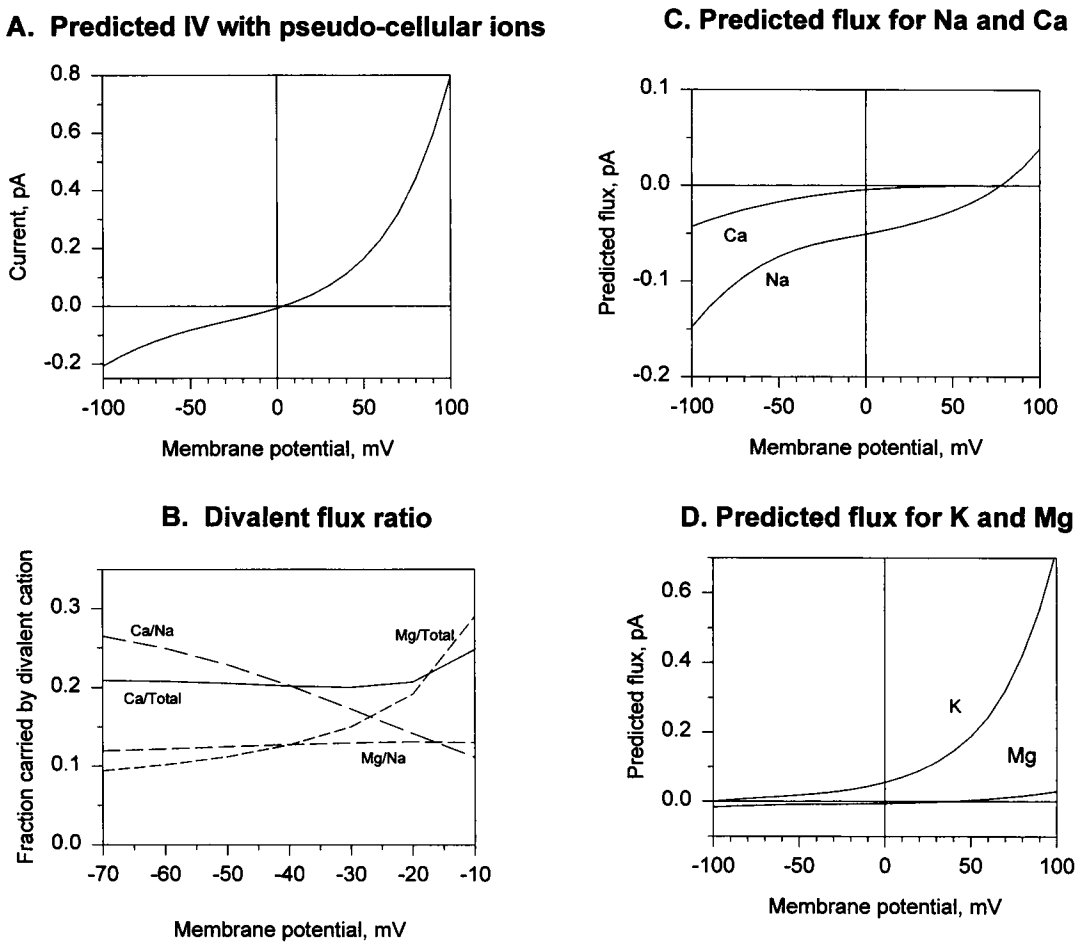

FIGURE 9 A predicted single-channel *IV* with pseudocellular ionic concentrations. A whole cell *IV* was predicted using ionic activities based on the following mM concentrations: $Na_i^+ = 6$, $Na_o^+ = 120$; $K_i^+ = 2.5$, $K_o^+ = 120$; $Ca_i^{2+} = 10^{-7}$ M, $Ca_o^{2+} = 1.5$; $Mg_i^{2+} = 0.3$, $Mg_o^{2+} = 6$. The outwardly rectifying *IV* has an E_{rev} of 3.44 mV, similar to that seen in intact rods. (*B*) Ca^{2+} and Mg^{2+} currents in pseudocellular solutions. The amount of current carried by either Ca^{2+} or Na^+ was divided by the amount of current carried by Na^+ or the total current and plotted as a function of potential. The fraction of total current carried by Ca^{2+} is 21% between −70 and −20 mV. (*C* and *D*) Predicted ionic flux versus voltage for each ion, based on pseudocellular ionic concentrations. The fluxes of the individual ions are calculated as described for Eq. 8. These fluxes combine to form the predicted cellular *IV* in Fig. 9 *A*.

ulated by the β subunit, cell regulatory mechanisms, or posttranslational modifications of the channel, which differ between photoreceptor patches and heterologous expression of CNGCs.

Second, the model predicts that permeability ratios determined from single-sided Ca^{2+} or Mg^{2+} addition depend on the concentration of the divalent cation. The magnitude of the dependence is small, however, and probably experimentally detectable only at divalent concentrations greater than 10 mM. Concentration-dependent permeability ratios with single-sided addition are not a distinguishing feature of a multisite channel, however, because it also is a feature of single-site Eyring models with asymmetrical energy profiles (Eisenman and Horn, 1983). The subtle concentration dependence predicted below 10 mM divalent ion activities is consistent with the single permeability ratio model previously used to interpret data with these ions (Picones and Korenbrot, 1995). An experimental test of the model predictions for concentration-dependent permeability ratios would employ a range of divalent activities larger than 10 mM with single-sided addition protocols.

Third, AMF effects for Na^+, K^+, Ca^{2+}, and Mg^{2+} are only predicted with a limited set of conditions of ionic concentration and often with either E_{rev} or conductance but not both measurements. For the most part, the concentrations predicted to show AMF effects are outside the range of typical experiments with these ions. In addition, the magnitude of the effects on E_{rev} and conductance are small and not easy to determine experimentally with a high degree of confidence. These factors would contribute to the difficulty of demonstrating AMF effects with these ions, as suggested by results from a number of laboratories (Haynes, 1995a; Sesti et al., 1995; Zimmerman and Baylor, 1992; Menini, 1990). The limited set of conditions under which AMF effects are predicted with our two-site model also serve as a reminder that the absence of AMF effects under particular

experimental conditions is not strong support for a single-site model of cationic permeation through the retinal rod CNGC.

Fourth, a useful permeation model will enable us to better understand Ca^{2+} influx, Ca^{2+} competition within the pore, and effects of other physiological ions such as Mg^{2+} (Hurwitz et al., 1995). The very small Ca^{2+} currents in photoreceptor rod CNGCs have been difficult to study experimentally, despite the physiological and biophysical significance of Ca^{2+} permeation in CNGCs. The agreement is noteworthy because the model was optimized from data with saturating amounts of cGMP, whereas a physiological amount of cGMP, less than 5 μM, was estimated from the experimental measurements (Yau and Nakatani, 1985b). The relative contributions of Ca^{2+} and Mg^{2+} to the total current, therefore, do not depend significantly on the level of cGMP, which agrees with the experimental finding that relative current block by Ca^{2+} and Mg^{2+} is largely independent of cGMP concentration (Karpen et al., 1993). The reasonably good agreement between the predicted and experimental estimates of the fraction of current carried by Ca^{2+} and Mg^{2+} suggest that the two-site model can be used to predict total current as well as the flux of individual ions under ionic conditions that are experimentally inaccessible but physiologically relevant.

The parameter set in Table 1 satisfactorily fits the range of experimental behaviors of the CNGCs presented in this paper. On that basis, we have used it to predict other behaviors. Because of the complexity of the model, however, the set of values in Table 1 is not unique in its ability to fit these data. Inclusion of data from additional experimental conditions such as other ion concentrations or the simultaneous inclusion of both Ca^{2+} and Mg^{2+} in the bath would further constrain the range of acceptable parameter values. Because a number of our conclusions are based on extrapolations from these parameters, a different parameter set may modify the conclusions. Future experiments can test the model predictions, and in turn, the data will enable us to further refine the model.

Multi-ion versus single-site models for CNGCs

A number of investigators have used single-site Eyring rate theory models to account for CNGC macroscopic data from rods with monovalent and divalent cations (Picones and Korenbrot, 1992; Menini, 1990; Sesti et al., 1995; Zimmerman and Baylor, 1992). Recently, Haynes (1995a,b) fitted single-channel data from multiple cone patches using a single-site model. The parameters of his model were similar to the parameters derived by Picones and Korenbrot (1995) from macroscopic data from both rods and cones. Overall, single-site models have been reasonably successful at predicting the shape of the *IV* curves under several experimental conditions. In addition, the single-site model was reasonably good at predicting the E_{rev} for biionic experiments, whereas a two-site, three-barrier model with single occupancy and a two-site, three-barrier, double-occupancy model did not improve the fit to the data (Haynes, 1995a).

Although single-site models appear adequate to explain some features of permeation in CNGCs, the use of a single-site model can be questioned on the basis of experimental evidence that the channel is a multi-ion pore. Electrophysiological behaviors, in general, that distinguish multiple occupancy from single occupancy include 1) concentration-dependent ion permeability ratios; 2) deviation from a Ussing flux ratio exponent of 1; and 3) anomalous mole fraction effects (Eisenman and Horn, 1983). The first behavior was demonstrated for cGMP-activated currents in photoreceptor patches (Furman and Tanaka, 1990), and recently, anomalous mole fraction effects with monovalent ions were reported for CNGCs expressed in oocytes (Sesti et al., 1995). To incorporate these qualitative effects of occupancy by multiple ions and to more accurately describe the behavior of the CNGC from retina, a model must include at least two sites. The actual number of binding sites (i.e., energy minima along the permeation path) and the maximum number of ions that can occupy the channel, however, remain unknown. Although our two-site model accounts for the range of data presented in this paper, permeation data alone are insufficient to determine a unique energy profile that correlates with the structure of the pore. In one sense, an Eyring model can be considered as a mathematical construction that duplicates the qualitative and quantitative behavior of ion permeation. In another sense, an Eyring model does mimic the real processes of ion entry into a channel, ion binding to regions within the channel, and ion transitions between binding sites. In so far as these processes correlate with the Eyring energy profile, Eyring modeling may guide our understanding of the physical properties of the permeation path.

What are the structural correlations of the permeation model of the rod CNGCs?

Recent experiments directed at understanding the structural basis for the ion selectivity properties of CNGCs have focused on the P region of the channel (Root and MacKinnon, 1993; Eismann et al., 1994; Park and MacKinnon, 1995; Frings et al., 1995). A glutamate residue at position 363 in this region has been shown to affect divalent block and ion selectivity. Substitution of the glutamate by a neutral amino acid resulted in the loss of sensitivity to external divalent cations but not internal divalent cations (Root and MacKinnon, 1993). One explanation for these observations is that the channel has multiple binding sites, each predominately regulating block from one side of the channel. Eismann et al. (1994) also studied the effects of substituting Glu363 with other residues. Their results led to the realization that ion permeability and conductance are controlled by different residues in the pore because substitutions of Glu363 with other residues differentially affected these parameters. They suggest that Glu 363 is probably not the

selectivity filter for the permeation pathway in CNGCs, but may bind ions entering the lumen from the external surface. In another study involving Glu363, Park and MacKinnon (1995) examined divalent selectivity of the wild-type CNGC and demonstrated a relative affinity of $Ca^{2+} > Mg^{2+} = Sr^{2+} = Ba^{2+}$. Ca^{2+} was the only ion in the series that blocked with a Hill coefficient greater than 1, suggesting multiple binding sites. When Glu363 was substituted with Asp, the affinities of the divalents increased and the selectivity sequence changed to $Ca^{2+} > Sr^{2+} > Ba^{2+} > Mg^{2+}$, offering further support for the idea that Glu363 helps regulate divalent selectivity in retina CNGCs.

A recent study by Frings et al. (1995) compares the calcium permeation properties of heterologously expressed rod, cone, and olfactory CNGCs. These channels exhibit different P_{Ca}/P_K values of 1.7, 8.0, and 4.6 for rod, cone, and olfactory channels, respectively, and 1.9, 6.6, and 8.8 for P_{Mg}/P_K. They also determined the fraction of current carried by Ca^{2+} to be 0.25% for retina, 5.8% for cone, and 3.9% for olfactory CNGCs expressed in *Xenopus* oocytes at 0.3 mM Ca_o^{2+}. Although they were unable to determine the fraction of current carried at physiological concentrations of Ca^{2+} for rod and cone channels, olfactory channel current is carried almost entirely by Ca^{2+} above 3 mM Ca_o^{2+}. It is worth noting that all three channels have a glutamate residue in position 363, so the differences in relative permeabilities cannot be attributed to this residue alone.

Permeation modeling of wild-type and mutated forms of the CNGCs eventually may reveal energetic features of the pore that can be correlated with pore residues. Work with the Shaker K^+ channel has resulted in a proposed structural correspondence between residues in the pore domain and ion binding sites based on permeation properties (Perez-Cornejo and Begenisich, 1994). A four-barrier, three-site permeation model was used to simulate permeation data, and then the positions of the barriers and binding sites were aligned to a proposed β-barrel structural model of the pore region.

Another approach to correlating channel structure with function involves the use of model helical peptides that form ion channels in planar lipid bilayers (Kienker and Lear, 1995; Kienker et al., 1994). *IV* curves from helical 21-residue peptides with the sequence Ac-$(LSSLLSL)_3$-$CONH_2$ were determined in a range of ionic conditions. Neither a simple Nernst-Planck electrodiffusion model nor a multi-ion state transition model satisfactorily fit the *IV* curves over the full range of experimental conditions, underscoring the complexity of ion behaviors within a protein pore. Although permeation models should not be expected to lead directly to structural models of pore, the combination of approaches including site-directed mutagenesis, electrophysiological recording of single-channel and macroscopic currents, and model peptides can be expected to lead to a better understanding of the energetics of ion entry into the pore, ion interactions with residues within the pore, and ion-ion interactions within the pore.

The authors thank Drs. Sarah Garber, Dick Horn, and Jim Lear for helpful comments on the manuscript and Dr. Bob French for useful discussions about selectivity and permeation modeling. Inquiries about the modeling calculations can be directed to the authors at wells@athens.dental.upenn.edu.

REFERENCES

Alvarez, O., A. Villarroel, and G. Eisenman. 1992. Calculation of ion currents from energy profiles and energy profiles from ion currents in multibarrier, multisite, multioccupancy channel model. *Methods Enzymol.* 207:816–854.

Begenisich, T. B., and M. D. Cahalan. 1980. Sodium channel permeation in squid axons. I. Reversal potential experiments. *J. Physiol. (Lond.).* 307:217–242.

Bradley, J., J. Li, N. Davidson, H. A. Lester, and K. Zinn. 1994. Heteromeric olfactory cyclic nucleotide-gated channels: a subunit that confers increased sensitivity to cAMP. *Proc. Natl. Acad. Sci. USA.* 91: 8890–8894.

Butler, J. N. 1968. The thermodynamic activity of calcium ion in sodium chloride-calcium chloride electrolytes. *Biophys. J.* 8:1426–1433.

Campbell, D. L., R. L. Rasmusson, and H. C. Strauss. 1988. Theoretical study of the voltage and concentration dependence of the anomalous mole fraction effect in single calcium channels. *Biophys. J.* 54:945–954.

Chen, T. Y., Y. W. Peng, R. S. Dhallan, B. Ahamed, R. R. Reed, and K. Yau. 1994. A new subunit of the cyclic nucleotide-gated cation channel in retinal rods. *Nature.* 91:11757–11761.

Colamartino, G., A. Menini, and V. Torre. 1991. Blockage and permeation of divalent cations through the cyclic GMP-activated channel from tiger salamander retinal rods. *J. Physiol. (Lond.).* 440:180–206.

Cooper, K. E., P. Y. Gates, and R. S. Eisenberg. 1988. Diffusion theory and discrete rate constants in ion permeation. *J. Membr. Biol.* 106:95–105.

Eisenman, G., and R. Horn. 1983. Ionic selectivity revisited: the role of kinetic and equilibrium processes in ion permeation through channels. *J. Membr. Biol.* 76:197–225.

Eismann, E., F. Muller, S. H. Heinemann, and U. B. Kaupp. 1994. A single negative charge within the pore region of a cGMP-gated channel controls rectification, Ca^{2+} blockage, and ionic selectivity. *Proc. Natl. Acad. Sci. USA.* 91:1109–1113.

Eyring, H. 1935. The activated complex in chemical reactions. *J. Chem. Phys.* 3:107–115.

Eyring, H., R. Lumry, and J. W. Woodbury. 1949. Some applications of modern rate theory to physiological systems. *Record Chem. Prog.* 10: 100–114.

Forsythe, G. E., M. A. Malcolm, and C. B. Moler. 1976. Computer Methods for Mathematical Computations. Prentice-Hall, Englewwod Cliffs, NJ.

Frings, S., R. Seifert, M. Godde, and U. B. Kaupp. 1995. Profoundly different calcium permeation and blockage determine the specific function of distinct cyclic nucleotide-gated channels. *Neuron.* 15:169–179.

Furman, R. E., and J. C. Tanaka. 1990. Monovalent selectivity of the cyclic guanosine monophosphate-activated ion channel. *J. Gen. Physiol.* 96: 57–82.

Goulding, E. H., G. R. Tibbs, D. Kiu, and S. A. Siegelbaum. 1993. Role of H5 domain in determining pore diameter and ion conductance through cyclic nucleotide-gated channels. *Nature.* 364:61–64.

Haynes, L. W. 1995a. Permeation of internal and external monovalent cations through the catfish cone photoreceptor cGMP-gated channel. *J. Gen. Physiol.* 106:485–505.

Haynes, L. W. 1995b. Permeation and block by internal and external divalent cations of the catfish cone photoreceptor cGMP-gated channel. *J. Gen. Physiol.* 106:507–523.

Haynes, L. W., A. R. Kay, and K.-W. Yau. 1986. Single cyclic GMP-activated channel activity in excised patches rod outer segment membrane. *Nature.* 321:66–70.

Hille, B. 1975. Ionic selectivity, saturation, and block in sodium channels. *J. Gen. Physiol.* 66:535–560.

Hille, B. 1992. Ionic Channels of Excitable Membranes. Sinauer Associates, Sunderland, MA.

Hille, B., and W. Schwarz. 1978. Potassium channels as multi-ion single-file pores. *J. Gen. Physiol.* 72:409–442.

Hurwitz, R. L., D. Srivastava, and M. Y. Hurwitz. 1995. Channel structure and divalent cation regulation of phototransduction. *Behav. Brain Sci.* 18:478

Ildefonse, M., and N. Bennett. 1991. Single-channel study of the cGMP-dependent conductance of rods from incorporation of native vesicles into planar lipid bilayers. *J. Membr. Biol.* 123:133–147.

Jencks, W. P. 1987. General Acid-Base Catalysis. Dover Publications, New York. 190.

Karpen, J. W., R. L. Brown, L. Stryer, and D. A. Baylor. 1993. Interactions between divalent cations and the gating machinery of cyclic GMP-activated channels in salamander retinal rods. *J. Gen. Physiol.* 101:1–25.

Kaupp, U. B. 1991. The cyclic nucleotide-gated channels of vertebrate photoreceptors and olfactory epithelium. *Trends Neurol. Sci.* 14: 150–157.

Kaupp, U. B., and K.-W. Koch. 1992. Role of cGMP and Ca^{2+} in vertebrate photoreceptor excitation and adaptation. *Annu. Rev. Physiol.* 54:153–175.

Kienker, P. K., W. F. DeGrado, and J. D. Lear. 1994. A helical-dipole model describes the single-channel current rectification of an uncharged peptide ion channel. *Proc. Natl. Acad. Sci. USA.* 91:4859–4863.

Kienker, P. K., and J. D. Lear. 1995. Charge selectivity of the designed uncharged peptide ion channel Ac-$(LSSLLSL)_3$-$COHN_2$. *Biophys. J.* 68:1347–1358.

Levitt, D. G. 1978. Electrostatic calculations for an ion channel. I. Energy and potential profiles and interactions between ions. *Biophys. J.* 22: 209–219.

Lewis, C. A. 1979. Ion-concentration dependence of the reversal potential and the single channel conductance of ion channels at the frog neuromuscular junction. *J. Physiol. (Lond.).* 286:417–445.

Liman, E. R., and L. B. Buck. 1994. A second subunit of the olfactory cyclic nucleotide-gated channel confers high sensitivity to cAMP. *Neuron.* 13:611–621.

Marquardt, D. 1963. An algorithm for least-squares estimation of nonlinear parameters. *J. Appl. Math.* 11:431–441.

Matthews, G. 1986. Comparison of the light-sensitive and cyclic GMP-sensitive conductances of the rod photoreceptor: noise characteristics. *J. Neurosci.* 6:2521–2526.

Menini, A. 1990. Currents carried by monovalent cations through cyclic GMP-activated channels in excised patches from salamander rods. *J. Physiol. (Lond.).* 424:167–185.

Moore, J. W., and R. G. Pearson. 1981. Kinetics and Mechanism. John Wiley and Sons, New York. 166–172.

Nakatani, K., and K.-W. Yau. 1988. Calcium and magnesium fluxes across the plasma membrane of rod outer segment. *J. Physiol. (Lond.).* 395: 695–729.

Nizzari, M., F. Sesti, M. T. Giraudo, C. Virginio, A. Cattaneo, and V. Torre. 1993. Single-channel properties of cloned cGMP-activated channels from retinal rods. *Proc. R. Soc. Lond. B.* 254:69–74.

Park, C., and R. MacKinnon. 1995. Divalent cations selectivity in a cyclic nucleotide-gated ion channel. *Biochemistry.* 34:13328–13333.

Perez-Cornejo, P., and T. Begenisich. 1994. The multi-ion nature of the pore in Shaker K^+ channels. *Biophys. J.* 66:1929–1938.

Perry, R. J., and P. A. McNaughton. 1991. Response properties of cones from the retina of the tiger salamander. *J. Physiol. (Lond.).* 433: 561–587.

Picones, A., and J. I. Korenbrot. 1992. Permeation and interaction of monovalent cations with the cGMP-gated channel of cone photoreceptors. *J. Gen. Physiol.* 100:647–673.

Picones, A., and J. I. Korenbrot. 1995. Permeability and interaction of Ca^{2+} with cGMP-gated ion channels differ in retinal rod and cone photoreceptors. *Biophys. J.* 69:120–127.

Robinson, R. A., and R. H. Stokes. 1968. Electrolyte Solutions. Butterworths, London. 476–509.

Root, M. J., and R. MacKinnon. 1993. Identification of an external divalent cation-binding site in the pore of a cGMP-activated channel. *Neuron.* 11:459–466.

Sesti, F., E. Eismann, U. B. Kaupp, M. Nizzari, and V. Torre. 1995. The multi-ion nature of the cGMP-gated channel from vertebrate rods. *J. Physiol. (Lond.).* 487:17–36.

Sesti, F., M. Nizzari, and V. Torre. 1996. Effect of changing temperature on the ionic permeation through the cyclic GMP-gated channel from vertebrate photoreceptors. *Biophys. J.* 70:2616–2639.

Sesti, F., M. Straforini, T. D. Lamb, and V. Torre. 1994. Gating, selectivity and blockage of single channels activated by cyclic GMP in retinal rods of the tiger salamander. *J. Physiol. (Lond.).* 472:203–222.

Tanaka, J. C., and R. E. Furman. 1993. Divalent effects on cGMP-activated currents in excised patches from amphibian photoreceptors. *J. Membr. Biol.* 131:245–256.

Woodhull, A. M. 1973. Ionic blockage of sodium channels in nerve. *J. Gen. Physiol.* 61:687–708.

Yau, K. 1991. Calcium and light adaptation in retinal photoreceptors. *Curr. Opin. Neurobiol.* 1:252–257.

Yau, K., and T. Chen. 1995. Cyclic nucleotide-gated channels. *In* Handbook of Receptors and Channels. CRC Press, Boca Raton, FL. 307–335.

Yau, K., and K. Nakatani. 1985a. Light-induced reduction of cytoplasmic free calcium in retinal rod outer segment. *Nature.* 313:579–582.

Yau, K., and K. Nakatani. 1985b. Light-suppressible, cyclic GMP-sensitive conductance in the plasma membrane of a truncated rod outer segment. *Nature.* 317:252–255.

Yau, K.-W., and D. A. Baylor. 1989. Cyclic GMP-activated conductance of retinal photoreceptor cells. *Annu. Rev. Neurosci.* 12:289–327.

Yau, K.-W., L. W. Haynes, and K. Nakatani. 1986. Roles of calcium and cyclic GMP in visual transduction. *Fortschr. Zool.* 33:343–366.

Zagotta, W. N., and S. A. Siegelbaum. 1996. Structure and function of cyclic nucleotide-gated channels. *Annu. Rev. Neurosci.* 19:235–263.

Zimmerman, A. L., and D. A. Baylor. 1986. Cyclic GMP-sensitive conductance of retinal rods consists of pores. *Nature.* 321:70–72.

Zimmerman, A. L., and D. Baylor. 1992. Cation interactions within the cyclic GMP-activated channel of retinal rods from the tiger salamander. *J. Physiol. (Lond.).* 449:759–783.